Journal of Applied Fluid Mechanics, Vol. 19, No. 1, pp. 3368-3384, 2026. Available online at www.jafmonline.net, ISSN 1735-3572, EISSN 1735-3645. https://doi.org/10.47176/jafm.19.1.3568



Multi-bubble Formation and Pressure Characterization under Mixed Injection Conditions

S. S. Lu¹, K. H. Xin¹, C. Dang², and H. W. Jia^{1†}

¹ College of Environmental Science and Engineering, Donghua University, Shanghai 201620, China ² Beijing Key Laboratory of Flow and Heat Transfer of Phase Changing in Micro and Small Scale, Beijing 100044, China

†Corresponding Author Email: jiahw@dhu.edu.cn

ABSTRACT

This study investigates the bubble formation process and the associated pressure fluctuation characteristics under mixed injection conditions. The experimental findings demonstrate distinct bubble generation modes depending on the syringe size. Specifically, when employing a syringe with an inner diameter (I.D.) of 0.6 mm, no significant liquid level lowering is observed in the syringe, and bubble formation occurs exclusively in a dripping type. In contrast, when utilizing a 0.9-mm I.D. syringe, the bubble formation process exhibits a transitional behavior, initiating in a jetting type before transitioning to a dripping type. This transitional behavior, termed the jetting-to-dripping type, is characterized by an obvious lowering of the gasliquid interface in the syringe. This study presents the development and validation of two distinct theoretical models to elucidate the pressure variations associated with bubble generation modes: the drip model and the jet model. The drip model demonstrated exceptional predictive accuracy in describing pressure characteristics during dripping-type bubble formation, showing remarkable congruence with experimental observations. In contrast, the jet model effectively captured the pressure fluctuation patterns associated with jetting-type bubble formation. Both models underwent validations across diverse experimental conditions, including variations in gas and liquid types, consistently demonstrating good predictive performance. Furthermore, the investigation systematically evaluated the influences of various parameters, specifically the gas chamber volume and gas supply rate, on the pressure dynamics during bubble formation. These findings provide valuable insights for the precise control and optimization of bubble generation processes in various scientific and industrial applications.

Article History

Received April 5, 2025 Revised July 11, 2025 Accepted August 5, 2025 Available online November 5, 2025

Keywords:

Pressure fluctuation Bubble generation modes Dripping-type Jetting-to-dripping type Distinct theoretical models

1. Introduction

Bubbles play a pivotal role in heat and mass across various domains, including manufacturing (Quan et al., 2025), agriculture (Wei et al., 2025), medicine (Shahidani et al., 2024), and chemical engineering (Fu et al., 2025). For instance, the injection of carbon dioxide bubbles into magnesium melts has not only enabled the efficient synthesis of graphene but also offered a solution for seawater pollution caused by oil spills (X. Li et al., 2022). Moreover, a novel electrolytic catalytic system (ECS) that harnesses nanobubble-contained electrolytic catalytic water (NECW) exhibits great potential for the remediation of petroleum hydrocarbon-contaminated soil

and groundwater (Ho et al., 2023). In metallurgical processes, the generation of gas bubbles is equally crucial. They not only facilitate chemical reactions but also contribute to the homogenization of the melt and the effective upwelling of impurities (Haas et al., 2021).

Given the significant role of bubbles in these fields, it becomes particularly essential to conduct in-depth studies on their generation mechanisms and kinetic properties. B. Yang et al. (2023) proposed a novel microelectrode bubble generator that successfully produced bubbles with diameters ranging from 0.4 to 1.4 mm and thoroughly discussed the mechanisms underlying the formation of individual and continuous bubbles. Guo et al. (2019) employed a microcellular foam

NOMENCLATURE			
r	bubble radial size	V_{b}	bubble volume
а	needle radius	h	height of syringe outlet from liquid level
Z	bubble height	i	time of bubble growth stage
P_{c}	chamber pressure	$ ho_{ m c}$	chamber density
$ ho_{ m b}$	bubble density	V_{c}	chamber volume
D	needle diameter	P_{b}	bubble pressure
$G_{\rm i}$	mass flow rate into the chamber	$Q_{ m i}$	volume flow rate into the chamber
P_0	initial pressure	$ ho_0$	initial density
γ	adiabatic index	Z	liquid level height in the syringe
σ	surface tension coefficient	ζ	local curvature
P_L	liquid pressure	$\mu_{ m l}$	liquid viscosity
$ ho_{ m l}$	liquid density	$\mu_{ m G}$	gas viscosity
$ ho_{ m G}$	gas density	P_{∞}	ambient pressure
ζ	ratio gas constant	R	Boltzmann's constant
$M_{ m mol}$	molar mass	m	gas mass flow in the syringe
$m_{\mathrm{c,i}}$	mass of gas in the chamber at moment i		

injection process, significantly enhancing the surface quality of foam parts through the bubble generation mechanism. Mei et al. (2023) investigated the bubble dynamics and mass transfer characteristics in petroleum-based liquids and proposed a new drag coefficient model applicable to such liquids. Zhou et al. (2021) targeted the performance of liquid fuel cells at high current densities and proposed the concept of a bubble trap layer to improve the stability of power generation. However, the current bubble generation technology still has several shortcomings. To address these problems, an in-depth examination of generation mechanisms and kinetic properties of bubbles has become particularly crucial.

The development of bubble generation techniques has provided new perspectives for research in related fields. Numerous scholars have attempted to optimize the bubble technology. Mohseni et al. (2023) achieved the periodic formation of sub-millimeter bubbles underwater through harmonic gas pressure modulation, thereby enhancing the reproducibility of bubbles. During the COVID-19 pandemic, a needleless injector technique based on thermal cavitation was proposed (González-Sierra et al., 2023). This technique utilizes thermal cavitation in a fused silica chamber to generate bubbles and achieves injection via a high-velocity jet. Bubble formation in submerged liquids is a common phenomenon in industrial processes, and orifice injection (Mohseni et al., 2022) and syringe injection (Mirsandi et al., 2020) are two widely adopted methods of bubble generation. Mirsandi et al. (2020) conducted an extensive analysis of orifice-generated bubble sizes, bubble growth mechanisms, and behavior of the contact line in the vicinity of an orifice by using a hydrophobic plate and an aqueous-ethanol solution to alter the wettability. Dzienis and Mosdorf (2023) carried out experimental and numerical studies on the variation of liquid pressure at the needle orifice during bubble generation, considering the effect of gas-liquid interfacial movement in the syringe on bubble generation.

Bubble generation modes can typically be classified into three types: constant pressure, constant flow, and mixed injection conditions, and the bubble generation mechanism corresponding to each mode has garnered extensive academic attention (J. Li et al., 2008; Kulkarni & Joshi, 2005; Krishnamurthi et al., 1968). Mi et al. (2019) investigated the effects of gas supply modes on the formation of N₂ bubbles in microfluidic T-structures under constant pressure and constant flow injection conditions. Davidson and Schüler (1997) incorporated a gas supply chamber in front of the injection needle tube to achieve the mixed injection condition. This design led to non-constant pressure in the gas supply chamber and varied flow rate into the bubbles. Goshima et al. (2022) designed a device for generating fine bubbles under an oscillating flow in the tube, where the chamber pressure was adjusted by a solenoid valve to control the bubblegenerating process during the mixed injection condition. Park et al. (1977) classified the air supply chamber into three types: small, medium, and large, and investigated the effect of chamber volume on bubble generation. Cano-Lozano et al. (2017) proposed an analytical model under mixed injection conditions, integrating the change in chamber pressure during the bubble formation stage, the water column evolution in the syringe after bubble detachment, and the subsequent increase in chamber pressure. Their final result showed a good agreement with experimental data (Zhang et al., 2017). Most current studies have focused on single bubbles, while fewer studies have discussed the more complex case of multiple bubbles.

Currently, few studies have investigated mixed injection, a condition that is frequently encountered in many industrial sectors. The primary objective of this study is to analyze the bubble formation process under mixed injection conditions, with particular focus on exploring the correlation between multiple bubble formation states and pressure changes in the supply chamber during a single pressure cycle. Through systematic experimentation and theoretical analysis, this study establishes fundamental principles governing bubble formation and develops a pressure variation model that accurately characterizes the formation process of different bubble types. Furthermore, this study comprehensively investigates the effects of key factors, including the inner diameter (I.D.) of the needle tube, the volume of the gas supply chamber, and the gas supply flow rate, on the bubble formation process.

2. EXPERIMENT

Deionized (DI) water, as well as 1 mmol/L and 10 mmol/L sodium dodecyl sulfate (SDS) solutions, were chosen as the continuous-phase liquid media for the experiments. N₂ and CO₂ gases were employed as the dispersed phases. The observation section was a square acrylic pipe with an inner size of 8 mm × 8 mm (shown in Fig. 1) and filled with liquid medium. A glass capillary tube, designed based on Dzienis et al. (2016), was used as the syringe for the experiments. Cylindrical acrylic chambers of different volumes (14,137 mm³, 37,868 mm³, and 50,265 mm³) were utilized to study the influence of chamber volume on the bubble generation and holding stages. The gas flow rate was controlled by a mass flow controller (Alicat, 0-100 mL/min), which ensured a flow range of 0-50 sccm. A filter was installed in front of the controller to prevent gas contamination. Sub-millimeter glass microelectrode tubes with an I.D. of 0.6, 0.8, 0.9, 1.1, and 1.2 mm manufactured by Nanjing Geology were used in the experiments (Mohseni et al., 2021; Oguz & Prosperetti, 1993). Bubble images were captured every 2 ms using a high-speed camera (Revealer) with a resolution of 720×828 pixels. The diameter of the syringe was used as a reference size, thus estimating the change in bubble volume over time, denoted as $V_b(t)$. To ensure the accuracy and analyzability of the images, the light source, the syringe port, and the high-speed camera were placed on the same level. Additionally, the axial symmetry of bubble formation was confirmed through the use of a prism. The contours of the bubbles were extracted from the captured images using MATLAB's edge recognition algorithm. The captured bubble image was binarized to identify the bubble edges, and the corresponding coordinate values were obtained using the bwboundaries function in MATLAB. After determining the bubble contour, the bubble volume could be

calculated considering the axisymmetric nature of the bubble, i.e., $V_b(t) = \int_0^{Z_{max}} \pi r^2(z)$. The pressure of the supply chamber was monitored by a high-frequency pressure sensor (HM90A) with a range of 0.2 MPa and an accuracy of 0.25%. Meanwhile, a data acquisition instrument (Agilent 34972A) was used to record the pressure change $P_c(t)$ with an interval of 10 ms. By combining the visualized bubble images and the pressure fluctuation data, this study aims to explore the pressure change patterns during the generation of bubble clusters of different morphologies and to analyze the underlying causes.

In this investigation, 3–5 replicate experiments were conducted for each operational condition, with data analyzed using mean values to ensure statistical reliability. Uncertainty analysis was performed during the calculation of bubble volumes, with the actual bubble volume error constrained within 5% when using the I.D. of the injection needle as the reference parameter.

3. BUBBLE GROUP MORPHOLOGY AND PRESSURE CHANGES

3.1 Bubble Group Morphology

Figure 2(a) shows the bubble morphology evolution during the injection of N_2 gas at a flow rate of 10 mL/min, with a gas chamber volume of 50,265 mm³ and a syringe I.D. of 0.6 mm. In the initial stage of bubble generation, the liquid level inside the syringe remains unchanged. That is, the gas-liquid interface stays stable, and this stage is termed the holding stage. Subsequently, the bubbles progress to the growth stage. During this period, the bubbles take on regular round or oval shapes and are produced independently, without undergoing bubble

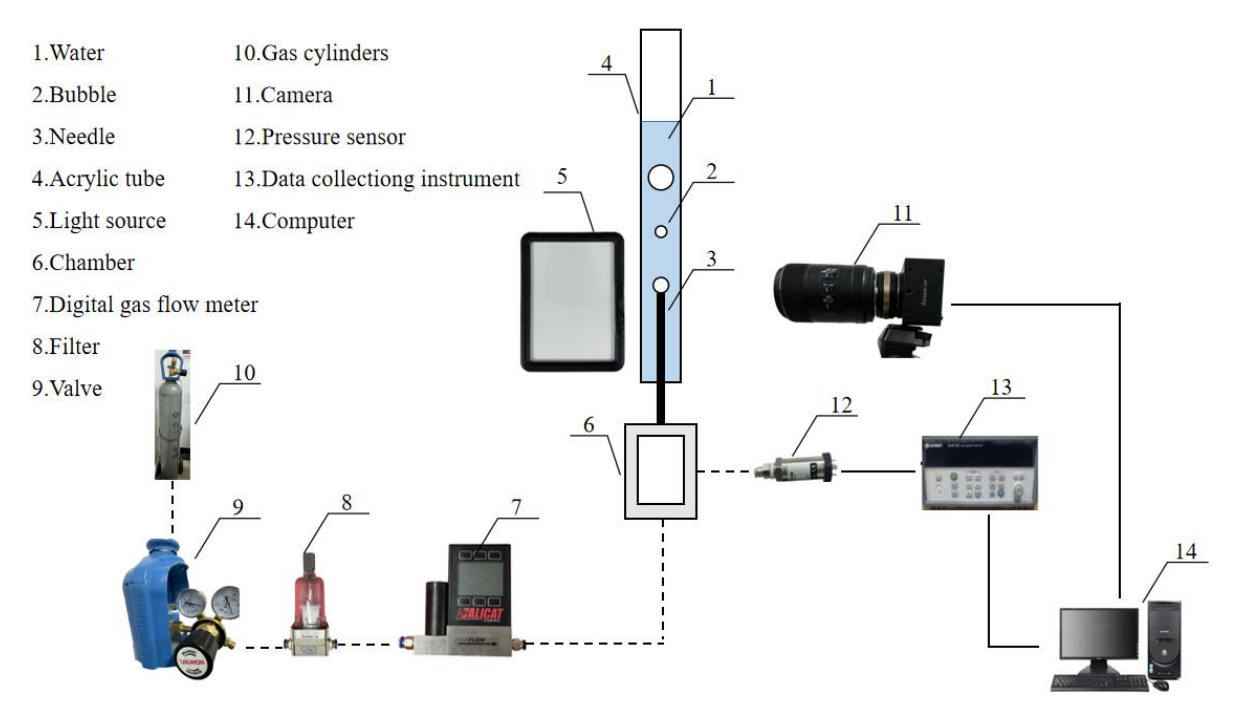


Fig. 1 Schematic diagram of the experimental system

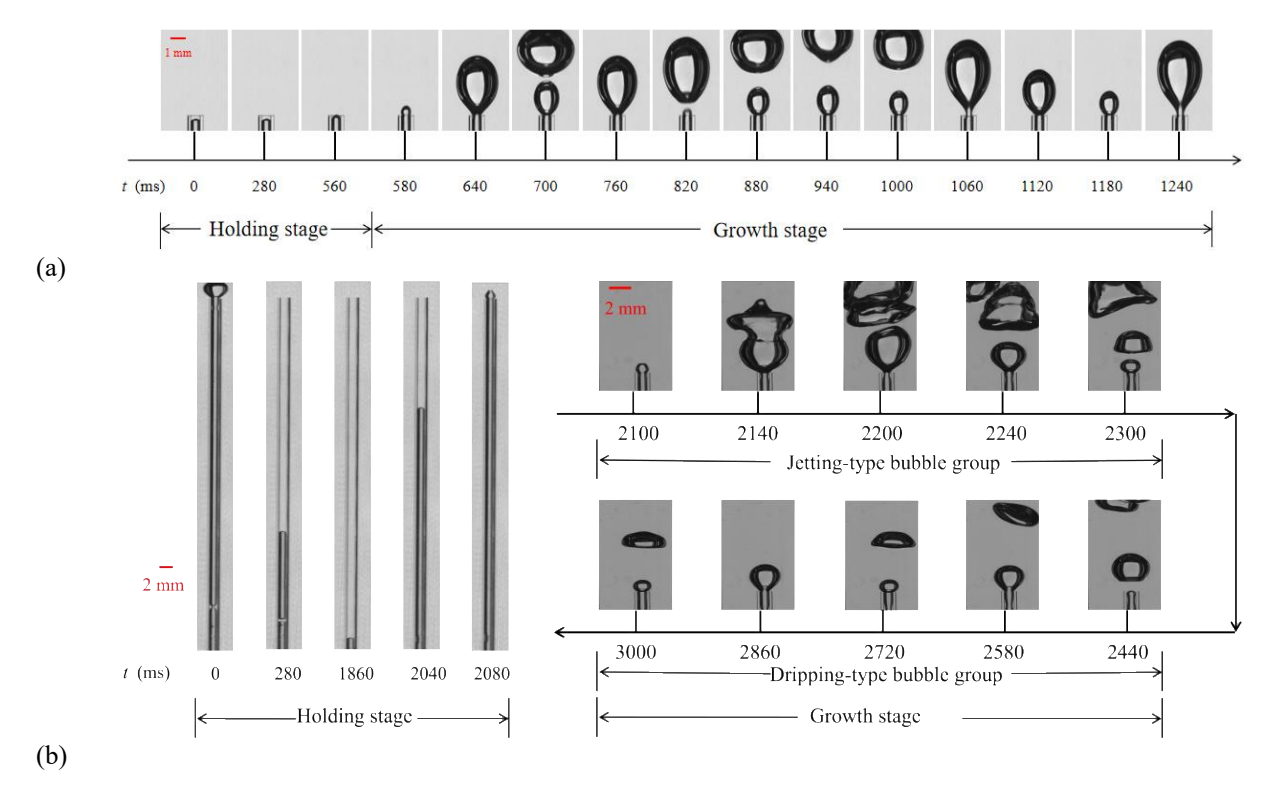


Fig. 2 (a) Dripping-type bubble generation and morphology change processes in the case of N_2 , D=0.6 mm, Q=10 mL/min, and $V_c=50,265$ mm³. (b) Changes in bubble morphology of the jetting-to-dripping type and lowering of the gas-liquid interface in the syringe in the case of N_2 , Q=20 mL/min, $V_c=50,265$ mm³, and D=0.9 mm

coalescence (Boubendir et al., 2020). The bubble formation process is a fluid-breaking process induced by interfacial instability, primarily driven by interfacial tension and shear force. In this process, the influence of inertial force is relatively minor (Yu et al., 2020). The release of bubbles from the needle tube is somewhat similar to the "dripping" phenomenon of a faucet (Ambravaneswaran et al., 2004). Given the continuous generation of discrete multiple bubbles in a single pressure cycle, this study categorizes the bubble formation process as a dripping-type bubble group.

Figure 2(b) illustrates the bubble morphology evolution during the injection of N_2 at a flow rate of 20 mL/min through a syringe with an I.D. of 0.9 mm. During the holding stage, a droplet of the liquid column in the syringe is observed. In the bubble growth stage, the gas-liquid interface rapidly ascends from the bottom to the top, generating a significant inertial force. This inertial force leads to the formation of jets and bubble coalescence, characterized as a jetting-type bubble group.

As bubbles are continuously released, the effect of the inertial force diminishes rapidly. Consequently, the driving pressure generated by the bubbles also decreases, leading to a transition in the bubble-generation mode from the jetting type to the dripping type, that is, the jetting-to-dripping type. It is worth noting that, although the generation of the jet bubble group also stems from interfacial instability-induced fluid fragmentation, the inertial force plays a more important role in the jetting process compared to the dripping-type bubble generation mode (M. Li et al., 2020).

3.2 Forms of Pressure Fluctuations

Figure 3 depicts the pressure fluctuations in the gas chamber for syringes of different I.D. values and various bubble-generation modes. During the holding stage, the gas chamber is continuously pressurized because bubbles have not yet formed at the syringe port. In the growth stage, the pressure in the gas chamber starts to gradually decrease as the bubbles are released. The experimental data reveal that the pressure exhibits an increasing trend during the holding stage, manifested in two forms: linear and non-linear increases. In the bubble-growth stage, the pressure drop also presents two scenarios: a rapid pressure drop and a pattern of rapid decrease followed by a slow decrease. These observations are consistent with the findings of Park et al. (1977). For gas-supply chambers and syringes of the same size, the "slowdecompression" process is more likely to occur under higher flow-rate conditions. Notably, during the holding stage, a significant drop in the liquid column is observed in the 0.9-mm I.D. syringe, but not in the 0.6-mm I.D. syringe. By examining the curves, we can see that the pressure change is closely associated with the bubbleformation process and the change in the liquid column in the syringe.

Compared to Fig. 3(c), Fig. 3(d) demonstrates that the pressure decreases slowly within a certain range, which is due to the production of continuous small dripping-type bubbles after the jetting-type bubbles (see Fig. 2(b) for details). In the early stage of the bubble group, the output flow rate is high, and the pressure decreases rapidly. In the later stages of the bubble group,

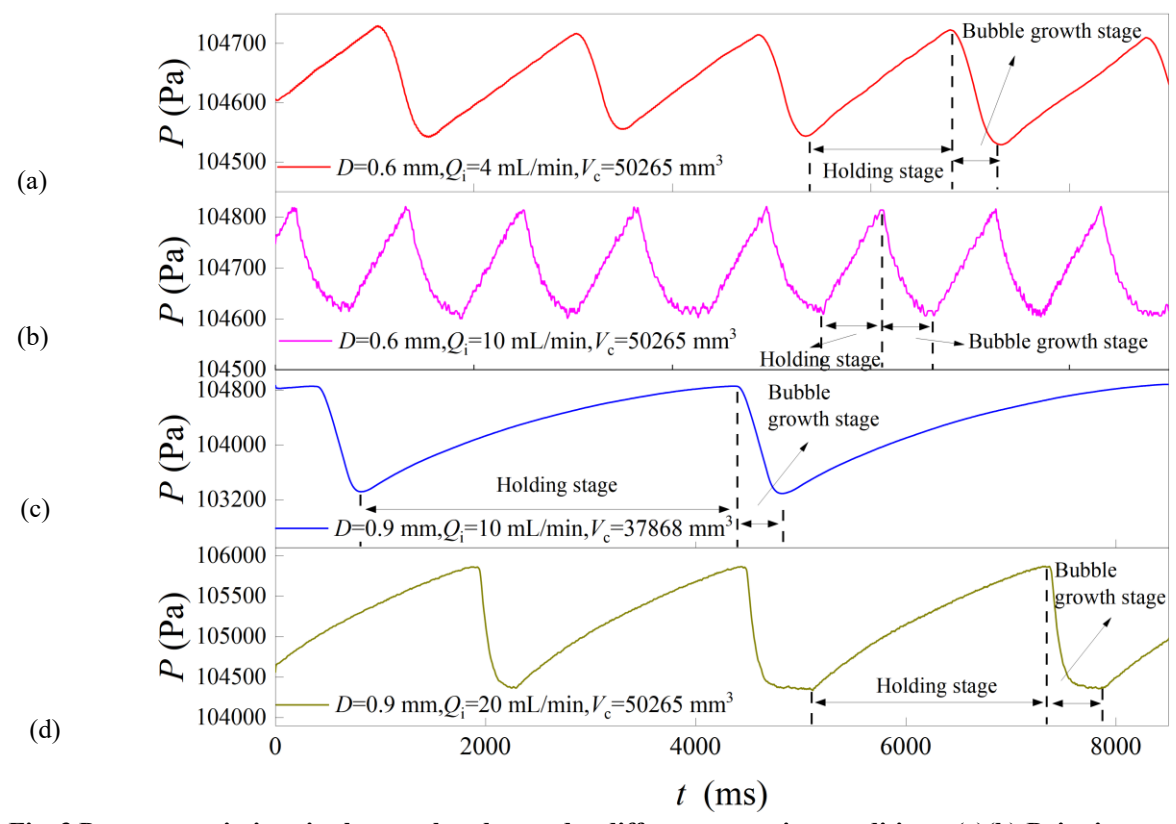


Fig. 3 Pressure variations in the gas chamber under different operating conditions. (a)(b) Dripping-type bubble group. (c)(d) Jetting-to-dripping-type bubble group

the flow rate of the output is smaller, and the gas flow rate in the output supply chamber approximates that of the input supply chamber, so the pressure fluctuation is approximately constant.

During the initial phase of the holding stage (i.e., following the previous bubble release cycle), variations in syringe I.D. cause the liquid level to either remain at the syringe mouth or retreat toward the gas-supply chamber. Continuous gas injection leads to a progressive pressure increase in the gas chamber. Once the gas chamber pressure reaches a threshold, the gas-liquid interface experiences rapid ascent to the needle opening. This process initiates bubble formation and marks the commencement of the bubble growth stage. In contrast, when there is no liquid column lowering in the syringe, bubbles will be generated and detached directly at the needle mouth, which is consistent with the capillary phenomenon observed by Xiang et al. (2022) and Zhao and Sun (2024).

To visualize the distribution of N_2 bubble-generation types under different working conditions, we summarize the data in Fig. 4(a). It is evident that when syringes with an I.D. of 0.6 mm and 0.8 mm are utilized, the bubble generation process predominantly adheres to the dripping type. Additionally, during the holding stage, no significant decline in the liquid column height in the syringe is observed. However, when using 0.9-mm and 1.1-mm syringes, the bubble generation pattern follows the jetting-to-dripping type as the I.D. increases or the flow rate decreases. In these cases, the holding stage is

accompanied by a drop in the liquid column inside the syringe.

Whether the liquid level in the syringe decreases seems to be the key feature to distinguish the dripping type and the jetting-to-dripping type. Figure 4(b) shows the force balance analysis of the gas-liquid interface, where $P_l + P_{\infty} = P_c + P_{\sigma}$. In the equation, $P_l = \rho_l g H$, and $P_{\sigma} = 2\sigma/\alpha$. σ represents the surface tension coefficient, and a is the inner radius of the syringe. It can be deduced that P_{σ} is inversely proportional to the syringe diameter D ($P_{\sigma} \propto 1/D$). P_{c} is the static pressure inside the supply chamber. Because the gas velocity u_i at the inlet of the supply chamber rapidly drops to zero upon entering the chamber, all the dynamic pressure is converted to static pressure. That is, P_c is proportional to the supplied gas momentum, i.e., $P_c \propto 0.5 \rho_i u_i^2$. Since the gas velocity at the inlet of the gas supply chamber is proportional to the injected flow rate $u_i \propto Q_i$, P_c is also proportional to the gas flow rate $(P_c \propto Q_i)$. A larger D and a smaller Q_i cause the gas-liquid interfacial force to become unbalanced. The downward pressure at the gasliquid interface is larger than the upward pressure, and the gas-liquid interface moves downward.

Figure 5 presents the amplitude of pressure fluctuations during the generation of N_2 bubbles in water under diverse operating conditions. For the 0.6-mm I.D. syringe, the pressure experiences relatively minor variations and shows little dependence on either the gas chamber volume or the supply flow rate. In contrast, for the 0.9-mm I.D. syringe, when a decrease in the gas-

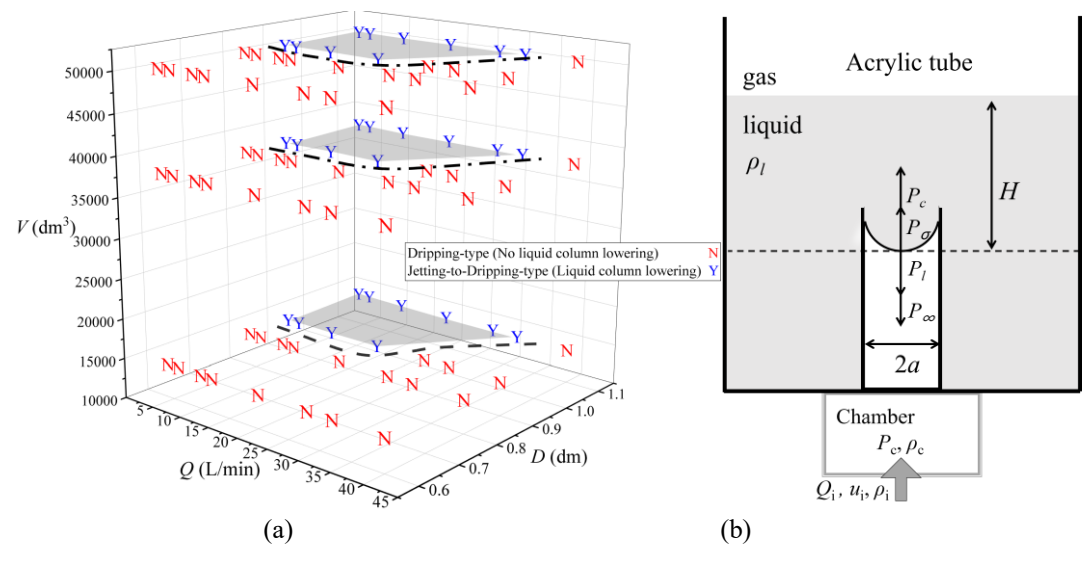


Fig. 4 (a) Correlation of gas flow rate, chamber volume, and needle I.D. with the generation mode of the bubble group. (b) Force analysis of the gas-liquid interface. P_l is the liquid pressure at the gas-liquid interface, P_{∞} is the ambient pressure, P_c is the pressure in the gas supply chamber, and P_{σ} is the surface tension

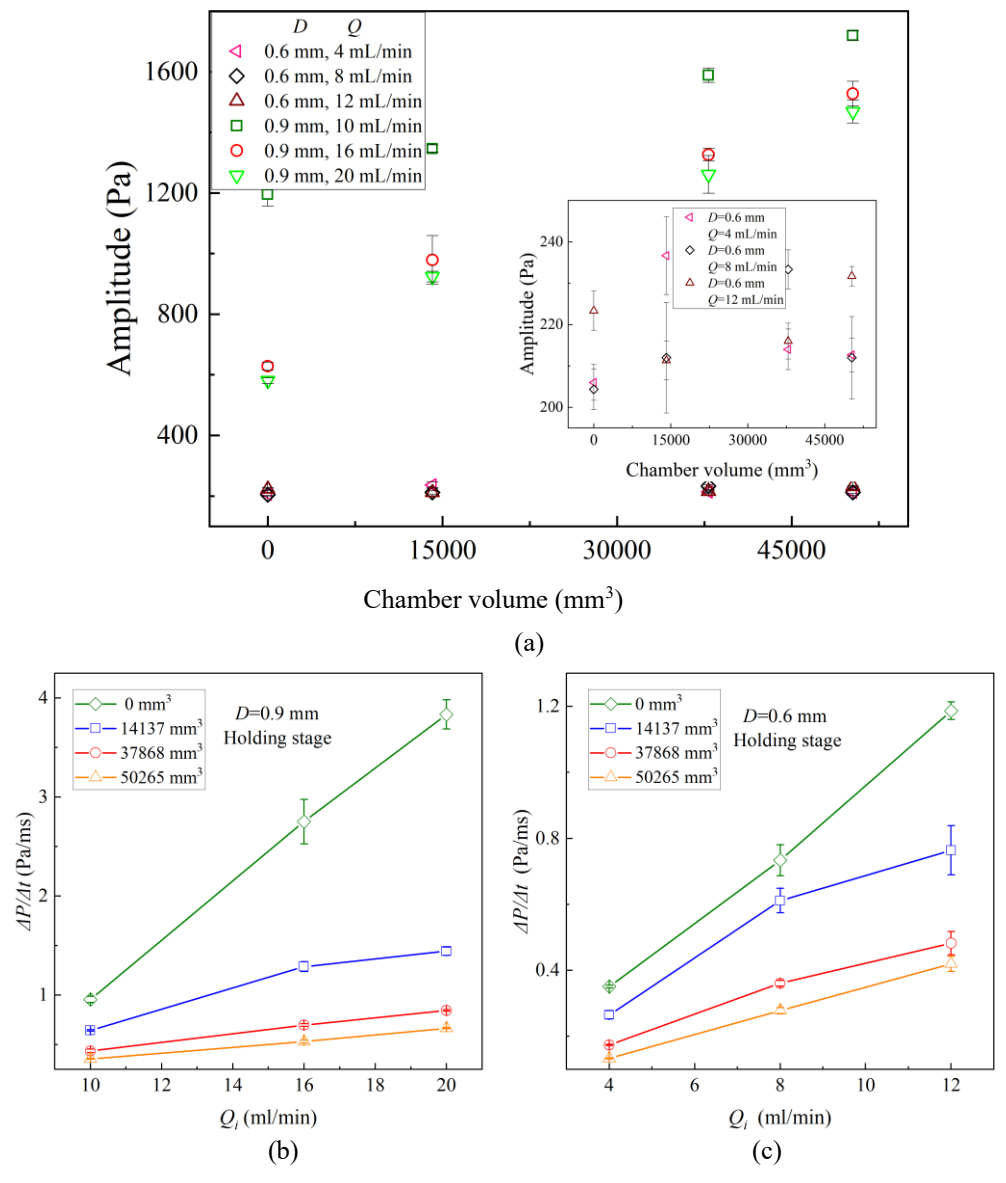


Fig. 5 (a) Effects of pipe diameter and flow rate size on the pressure amplitude in the holding stage for different chamber sizes. Effect of flow rate on the rate of pressure rise in the holding stage under (b) N_2 , D=0.9 mm, (c) N_2 , D=0.6 mm

liquid interface is observed, the amplitude of the pressure fluctuations increases with an increase in gas chamber volume. Simultaneously, the increase in gas chamber volume dampens the impact of the flow rate on the amplitude. For the same chamber volume, the amplitude of pressure fluctuations is significantly higher when the gas-liquid interface decreases compared to when it does not. Generally, the pressure amplitude of cases with a 0.9-mm I.D. syringe is larger than those with a 0.6-mm I.D. syringe. The descent of the gas-liquid interface to some extent reflects the "elasticity" of the system. Moreover, the flow rate would be another crucial factor. A lower flow rate implies that gas enters the supply chamber more slowly, so the gas-liquid interface in the syringe is more likely to drop. For both 0.9-mm and 0.6mm I.D. syringes, the rate of pressurization during the holding phase increases with increasing flow rate (see Figs. 5(b) and 5(c)). When the flow rates are equal, the smaller the air supply chamber volume, the faster the pressurization rate. For a small chamber, the pressure required to release the bubbles can be reached faster.

4. DRIP MODEL

Figure 6 presents the schematic of a physical model illustrating the process by which a syringe, equipped with a gas-supply chamber, releases gas bubbles in a liquid environment. In this model, the syringe is positioned at the bottom of the liquid chamber and connected to the gas supply chamber through a tube. This setup enables precise control and detailed observation of the bubble-release process, offering a visual aid for comprehending the physical mechanism of bubble generation. The radius and length of the syringe are a and L, respectively. The height and volume of the bubble change over time and are represented as z(t) and $V_b(t)$, respectively. The gas density inside the bubble is $\rho_b(t)$, and r denotes the radial dimension of the bubble. The volume of the gas supply chamber is V_c , and its internal pressure and gas density vary with time, denoted as $P_c(t)$ and $\rho_{\rm c}(t)$, respectively. The initial pressure is P_0 , and the initial density is ρ_0 .

It is assumed that the gas phase adheres to the idealgas behavior. Additionally, the gas pressure drop along the syringe is regarded as negligibly small compared to the pressure in the chamber. Consequently, the pressure drop along the syringe can be ignored, and we can approximate that $P=P_b$, and $\rho_c=\rho_b$.

Thus, applying the conservation of mass to the air supply chamber yields:

$$\frac{d[\rho_c(t)V_c]}{dt} = G_i - G_o(t) \tag{1}$$

where $G_i = \rho_0 \times Q_i$ is the mass flow rate injected into the gas chamber, ρ_0 is the gas density in the chamber after bubble release, $G_0(t)$ is the time-varying mass flow rate from the chamber to the bubbles, and $\rho_c(t)$ is the time-varying density in the supply chamber.

The following equation can be obtained by applying the mass conservation equation to bubbles:

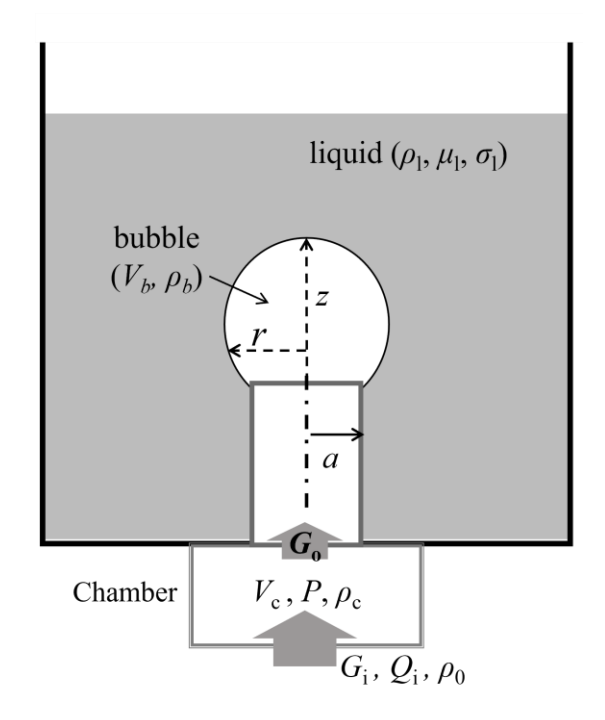


Fig. 6 Schematic diagram of the physical parameters. $P_c(t)$, $\rho_c(t)$, and $\rho_b(t)$ are the time-dependent gas pressure inside the chamber, the time-dependent density inside the chamber, and the time-dependent density inside the bubble, respectively

$$\frac{d\left[\rho_{\rm b}(t)V_b(t)\right]}{dt} = G_{\rm o}(t) \tag{2}$$

Combining the above two equations, we can obtain the following:

$$\frac{d[\rho_b(t)V_b(t) + \rho_c(t)V_c]}{dt} = G_i \tag{3}$$

When t=0, the bubble volume V_b is zero. From the above, it is known that $\rho_c=\rho_b$. Integrating the above equation, we obtain the gas chamber density over time:

$$\rho_c(t) = \rho_0 \left(\frac{V_c}{V_c + V_b(t)} \right) + \frac{G_i t}{V_c + V_b(t)}$$

$$\tag{4}$$

It can be seen from Eq. (4) that in the holding stage, since bubbles have not yet been generated (V_b =0), the gas density inside the chamber increases linearly with time, i.e., $\rho_c(t)$ = $\rho_0+G_t\times t/V_c$. During the subsequent bubble growth stage, $V_b(t)$ becomes prominent, and its value can be derived from the bubble image. The experimental outcomes for a syringe I.D. of 0.6 mm are presented in Figs. 3(a) and 3(b).

Finally, the variation of gas chamber pressure with time is obtained from the energy equation:

$$P_c(t) = \rho_c^{\gamma} \left(t \right) \left(\frac{P_0}{\rho_0^{\gamma}} \right) \tag{5}$$

where P_0 is the gas chamber pressure at the initial moment, and γ is the adiabatic index. N_2 is a diatomic gas with a degree of freedom at room temperature of 5

and an adiabatic index of γ =1.4 (Y. Yang et al., 2023). This model is employed to depict the pressure fluctuations in the holding stage and the bubble growth stage under the condition of no liquid-column reduction.

The pressure change in the gas chamber can be estimated by the above process, the so-called flow model, originally proposed by Cano-Lozano et al. (2017). This model is typically applied to cases with a constant contact angle. When the I.D. of the syringe is large, the model is no longer accurate due to the weakening of the capillary force effect as well as the dynamic change of the contact angle. In addition, in Cano-Lozano et al.'s experiments, a single pressure cycle produced only one bubble, whereas in the present study, multiple bubbles (i.e., a bubble group) may be formed during each pressure cycle Error! Reference source not found.. T herefore, the cumulative volume of released bubbles needs to be considered in the drip model for the pressure changes during bubble group formation, i.e., $V_b(t) = \sum V_b$, n (n=1, 2, 3...).

This research expands upon the single-bubble generation and pressure fluctuation model put forward by Cano-Lozano et al. The objective is to probe into the applicability of this expanded model when handling multiple-bubble generation scenarios in a pressure cycle. The remarkable consistency between model predictions and experimental observations, as illustrated in Fig. 7(a), further validates the efficacy of the drip model in the context of multiple-bubble generation.

The visualization outcomes reveal that the gasliquid interface remains intact throughout the experiment conducted in the 0.6 mm I.D. syringe, as depicted in Fig. 7(b). The green wireframe in Fig. 7(b) represents the bubble contour recognized by the MATLAB edge-detection algorithm. The drip model can precisely predict the pressure variation in the supply chamber under diverse flow-rate and supply-chamber-volume conditions when the bubble-generation process manifests a typical dripping-type mode, as shown in Fig. 7(b). For the dripping type, it is postulated that the pressure change in the air-supply chamber is principally induced by the disparity between the injected flow rate in the air-supply chamber and the output flow rate during the bubble-release moment.

To verify this hypothesis, this study monitored the temporal variation in the volume of each bubble within the bubble group and computed the input and output mass flow rates in the air-supply chamber (details are presented in Fig. 7(c2)). Under the experimental conditions illustrated in Fig. 7(a), Fig. 7(b) captures the morphology of the dripping-type bubble group through visualization techniques. These images enable the reader to intuitively comprehend the bubble-formation process. Figure 7(c1) elaborates on the temporal evolution of the volume of individual bubbles within the bubble group. Figure 7(c2) displays the data of the bubble-release flow rate versus the input flow rate to the supply chamber, revealing a crucial characteristic of the drip model during the buckling stage, namely, the imbalance between the input and output gas volumes. In the early stages of depressurization, the flow rate released by the bubbles

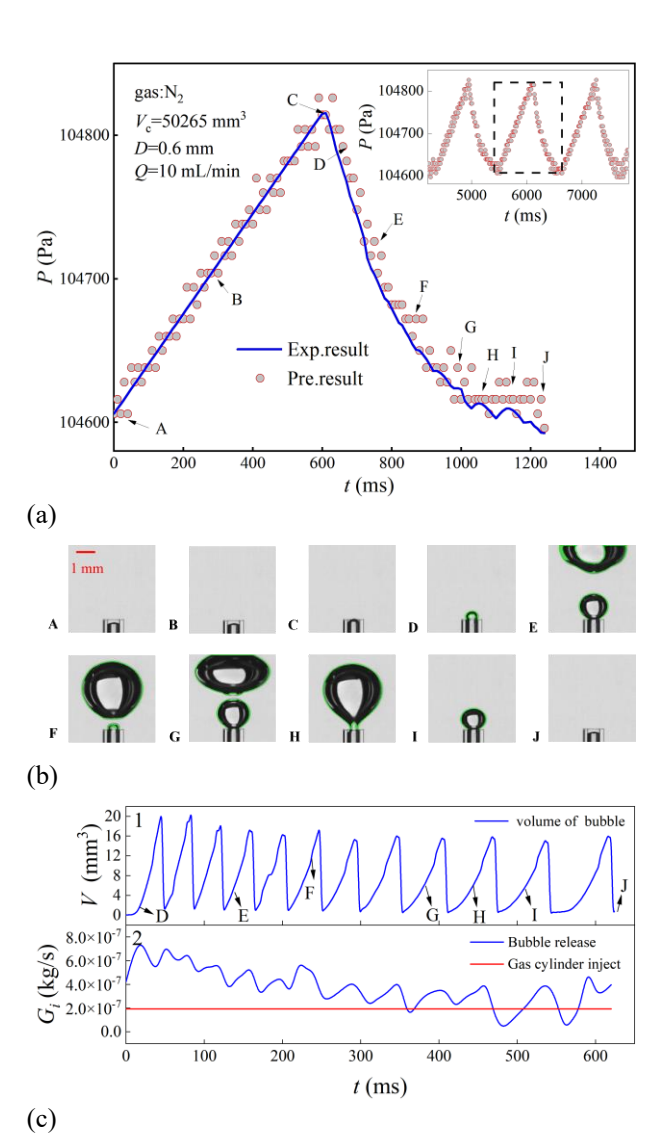


Fig. 7 Results in the case of N_2 , Q=10 mL/min, $V_c=50,265$ mm³. (a) Comparison of the drip model with experimental data. (b) Visualizations of the holding stage and the growth stage. (c1) Variation of the volume of each bubble in the bubble group with time. (c2) Mass flow rate of the injected gas into the chamber and the mass flow rate of the output gas

surpasses the input flow rate to the gas-supply chamber, leading to a pressure drop. As the process progresses, the release flow rate approaches the input flow rate, and the bubble release weakens correspondingly until the end of the release. In the initial stage, the bubbles grow in a jetting type and exhibit an approximately linear increase in volume size, but subsequently, the growth rate gradually decelerates. Specifically, a slight elevation in pressure fluctuations is observed at points H and I in Fig. 7(c1), and a slow initial volume expansion of the bubbles at points H and I is also noted. It is determined that the variation in the chamber pressure is associated with the change in the volume of the bubbles. At that moment, the volume of the output gas is smaller than the input volume ($dV_b/dt < G_i$) (shown in Fig. 7(c2)), which leads to an abnormal increase in the gas chamber pressure. Relatively, during the late stage of bubble growth, the gas chamber pressure shows a decreasing trend because the output gas flow rate is larger than the input flow rate (${\rm d}V_{\rm b}/{\rm d}t>{\rm G_i}$). These calculations not only support the hypothesis proposed above but also enhance the comprehension of the mechanism underlying the pressure change during the generation of dripping-type bubbles.

Figures 7(a), 8(a), and 8(b) illustrate that the experimental data chosen for comparison with the model are derived from stable periodic pressure fluctuations. This selection ensures the accuracy of the data and the reliability of the comparison when contrasted with the model. These data were gathered under diverse chamber volumes and flow conditions to validate the general applicability of the model in predicting the pressure in the air-supply chamber. As depicted in Figs. 7(a), 8(a), and 8(b), during each cycle of pressure change in the 0.6mm I.D. syringe, the observed bubble-generation process manifests as a dripping type. In this process, capillary pressure, surface tension, and shear are the primary factors influencing bubble generation. The abovementioned results confirm that the drip model is equally applicable in the scenario of multiple-bubble generation. The drip model can precisely predict the variation of gaschamber pressure within the dripping-type bubble group under different experimental conditions, where the capillary force plays a crucial role during the bubble growth stage. Consequently, for the dripping type, the drip model can accurately predict the pressure change in the gas chamber solely based on the bubble visualization images.

After summarizing the emergence patterns of various bubble-generation types, this study then analyzed the bubble visualization images in conjunction with the corresponding pressure data. Subsequently, a bubble physical model was developed to predict the pressure fluctuations during the generation of different patterns of bubbles. This would enrich the understanding of bubble formation dynamics and provide a potential prediction tool for the bubble generation process in engineering applications.

The experiment further expanded the research scope by employing carbon dioxide (CO2) as the gaseous species for the experiment. Figure 9(a) vividly depicts the process of CO2 bubble set generation in the dripping type. On this basis, Fig. 9(b) utilizes the drip model to predict the pressure changes in the gas chamber, and the results exhibit a high degree of consistency with the experimental data. This validates the applicability of the drip model for different gas types, suggesting that the model can yield accurate predictions as long as the bubblegeneration process adheres to the dripping type. By synthesizing Eqs. (1)-(5), we can see that in the drip model, the variation of gas species mainly plays a role by affecting the gas density factor, while the gas viscosity does not affect the prediction results of the model. Furthermore, when predicting the pressure fluctuations in the gas chamber with the drip model, the flow rate of the released gas is the primary factor. Notably, the alteration of gas species does not influence the calculation of this flow rate.

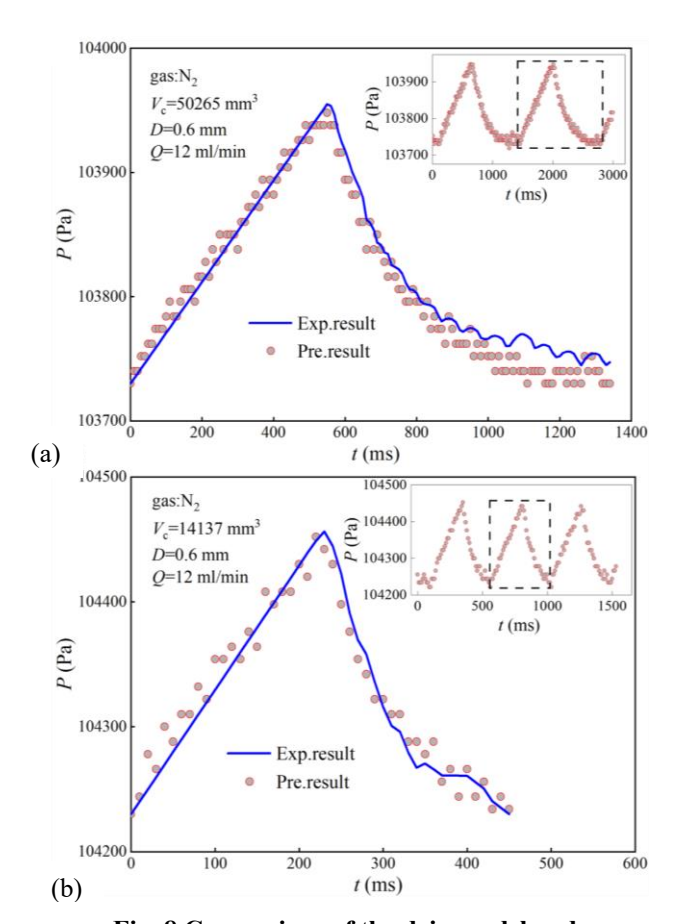


Fig. 8 Comparison of the drip model and experimental data under different operating conditions. (a) N₂, Q=12 mL/min, $V_c=50,265$ mm³, and D=0.6 mm. (b) N₂, Q=12 mL/min, $V_c=14,137$ mm³, and D=0.6 mm.

5. JET MODEL

comparing the pressure fluctuation characteristics of the jetting-to-dripping type and the dripping type, as presented in Fig. 3, it can be noted that during the holding stage, both modes show a similar upward pressure trend. Nevertheless, when entering the bubble growth stage, there is a significant difference in the dominant force between the two modes, which serves as the fundamental cause for the difference in the bubble formation mechanism. For bubbles in the jet model, the growth process is mainly controlled by inertial forces. Consequently, the original drip model, which is dominated by surface tension and shear forces, is no longer applicable at this stage. Additionally, when bubbles are released in a jet form, propelled by inertial forces, their volumes tend to be irregular. This irregularity presents a challenge to the accurate calculation of the bubble volume. As a result, it is not feasible to utilize the drip model to predict the pressure fluctuations during the growth stage of a jetting-todripping-type bubble group.

In the experimental results from the 0.9-mm I.D. syringe, as depicted in Figs. 3(c) and 3(d), the pressure during the holding stage does not exhibit a linear increase; instead, the pressure curve is slightly convex.

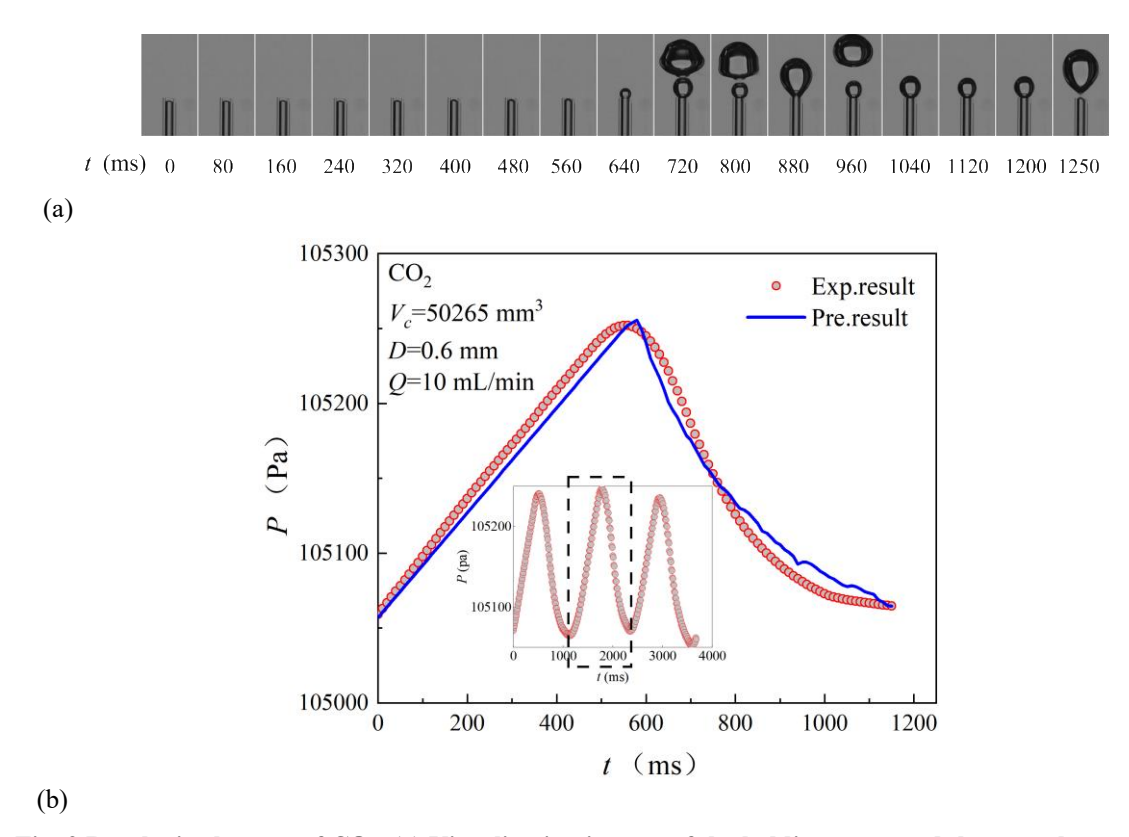


Fig. 9 Results in the case of CO₂. (a) Visualization images of the holding stage and the growth stage. (b)

Comparison of the pressure diagram and the drip model

Simultaneously, the position of the gas-liquid interface in the syringe undergoes significant alterations, suggesting that the influence of the water-column height in the syringe cannot be overlooked. Consequently, when considering the temporal variation of the gas-chamber density as the liquid level height in the syringe changes, denoted as Z(t), the following equation is derived from Eq. (4):

$$\rho_{c}(t) = \rho_{0} \left(\frac{V_{c}}{V_{c} + V_{b}(t) + \pi a^{2} Z(t)} \right) + \frac{G_{i}t}{V_{c} + V_{b}(t) + \pi a^{2} Z(t)}$$
(6)

Eq. (6) is employed to depict the pressure change during the holding stage of the jetting-to-dripping-type bubble group. In comparison with the drip model that does not account for the liquid-column reduction phenomenon, the influence of the liquid column is incorporated into Eq. (6).

During the bubble growth process, the flow in the syringe causes the pressure P_b inside the bubble to be lower than the filling-chamber pressure P_c . The liquid pressure P_L at the bubble interface is related to P_b , and the following relationship can be derived by performing a force balance analysis of the gas-liquid interface:

$$P_b = P_L + \sigma \xi \tag{7}$$

where σ is the surface tension coefficient, and ξ is the local curvature.

When the radius of curvature of the bubble growth is equivalent to the radius of the syringe, the interfacial tension is at its minimum. In other words, the gas-

chamber pressure reaches the minimum value at this point:

$$P_{c,\min} = P_{\infty} + 2\sigma/a \tag{8}$$

where P_{∞} is the ambient pressure. Here, it is considered that the pressure drop along the syringe is slow relative to $P_{\rm c}$, and the approximation as a Poiseuille flow is valid. Consequently, the following expression for the gas mass flow rate m can be derived:

$$\dot{m} = \frac{\pi}{8} \frac{\rho_G a^4}{\mu_G} \frac{dP}{dx} \tag{9}$$

where μ_G and ρ_G are the gas viscosity and density, respectively. In addition, under the assumption of isothermal flow, the gas equation of state is utilized to obtain $\rho_G = P_G/\zeta T$ ($\zeta = R/M_{mol}$, where ζ is the ratio gas constant, R is the Boltzmann's constant, and M_{mol} is the molar mass). Using the conservation of mass, the mass flow rate at a given moment i can be obtained as follows:

$$m_i = -\frac{RT\pi T^4 (P_i^2 - P_{\infty}^2)}{16M_{mol}V\mu\mu L\xi}$$
 (10)

Given that the interfacial tension is negligibly small compared to the pressure in the chamber, the magnitude of the tension is neglected. It is assumed that $P_{\infty} \approx P_{c,min}$ in the above equation. P_0 represents the maximum pressure in the holding stage, which is also the maximum pressure in the chamber.

Based on the conservation of mass in the chamber, the amount of change of mass inside the chamber at moment *i* can be obtained as follows:

$$\Delta G_i = m_i - G_i \tag{11}$$

where G_i is the gas flow into the chamber at moment i. G_0 equals $\rho_0 V_c$ at the initial moment. The pressure in the chamber at moment i can be further obtained through the gas equation of state:

$$P_i = \frac{m_{c,i}RT}{M_{mol}V_c} \tag{12}$$

Conservation of mass is performed for the chamber to obtain the gas mass $m_{c,i} = \rho_{i-1}V_c - \Delta G_i \Delta t$ inside the chamber. Bringing $m_{c,i}$ into Eq. (12) yields:

$$P_{i} = \frac{\left(\rho_{i-1}V - \Delta G_{i}\Delta t\right)RT}{M_{mol}V_{c}} \tag{13}$$

The gas density in the supply chamber at moment i can also be obtained from the gas equation of state:

$$\rho_i = \frac{M_{mol}P_i}{RT} \tag{14}$$

In the application of the jet model, the type of gas significantly affects the gas density and viscosity parameters. Given the high-velocity movement of the gas in the syringe, the viscosity parameter plays a vital role in the model. The study reveals the presence of two buckling stages, namely the fast and slow stages, of pressure fluctuations during bubble generation in the jetting model under jet-dominated flow. As the chamber volume increases, the slow buckling stage becomes more prominent, as can be seen from Figs. 10 and 11. Figure 10(a) further illustrates that in the 0.9-mm I.D. syringe, the rising time of the liquid column in the holding stage is shorter than the falling time. In the bubble growth stage, bubbles are first generated in the jetting type and then switched to the dripping type. The dropping phase in the pressure fluctuation cycle is mainly driven by the jet, with a sharp pressure drop in the gas-supply chamber during jetting-type bubble generation (for example, from E to G in Fig. 10(b)). In contrast, the pressure drop is relatively smooth during dripping-type bubble formation (e.g., from H to I in Fig. 10(c)).

In summary, a larger inertial driving force in the initial stage leads to the generation of jetting-type bubbles. With the release of the jet bubbles, the pressure in the air-supply chamber decreases dramatically, leading to a decrease in the driving pressure of subsequent bubbles, which transform into dripping-type bubbles. Consequently, it can be firmly concluded that jetting-type bubbles, engendered by inertial forces, give rise to a rapid pressure reduction phase in the supply chamber, whereas dripping bubbles induce a slow pressure reduction phase. Integrating the jet model and the drip model, the type of bubble growth can be predicted based on the pressure-fluctuation diagram (Ruiz-Rus et al., 2020).

Figures 10(c), 11(a), and 11(b) respectively present the pressure fluctuations in the supply chamber for N_2 and CO_2 at different chamber volumes compared with the jet

model. In the case of the 0.9-mm I.D. syringe, bubble generation is predominantly governed by the jet flow. The experimental data vividly illustrate that the agreement between the jet model results and the experimental data is quite high. As evident from Fig. 11(b), the model predicts a steeper downward trend during the bubble generation phase compared to the experimental data. This discrepancy underscores the inherent limitations of the model. The current jet model lacks sufficient consideration of local drag effects in the piping system, representing a key factor responsible for the observed deviation between model predictions and experimental results. Additionally, a comparative analysis of Figs. 11(a)–(b) and Fig. 10(c) reveals that the model exhibits significantly greater discrepancy from experimental data for CO₂ than for N₂. This disparity underscores the necessity for the jet model to explicitly incorporate the influence of gas solubility, as the dissimilar solvation behaviors of different gaseous species impact the model's prediction accuracy. To improve model accuracy and reliability, future research should focus on a comprehensive analysis and incorporation of these local drag factors. These enhancements will enable the model to better represent actual physical phenomena, thereby advancing related research and engineering applications.

6. BUBBLE GENERATION AND PRESSURE CHARACTERIZATION OF SDS SOLUTIONS

SDS is a typical anionic surfactant. Its critical micelle concentration (CMC) is about 8.2 mM/L, which means that it can decrease the surface tension of the solution at lower concentrations. The experimental protocol involved adding 1 mmol/L SDS surfactant to DI water, corresponding to 0.125 times the CMC. concentration was specifically chosen to maintain sub-CMC conditions, thereby preventing micelle formation and associated deposit effects. The resulting surface 31.2 approximately tension measured representing a reduction of approximately 50% compared to that (72 mN/m) of DI water. As illustrated in Fig. 12(b), the gas-liquid interface in the syringe exhibits characteristic rise and fall behavior in the presence of the surfactant. The gas-liquid interface undergoes acceleration during interface descent and experiences deceleration during the ascent phase. These observations show excellent agreement with the visualization results shown in Fig. 12(a). This observed behavior correlates precisely with the trend shown in Fig. 12(c), wherein the gas-supply chamber pressure undergoes a rapid initial increase during the ramp-up phase, subsequently transitioning to a gradual ascent. When using DI water, the 1.2-mm I.D. syringe exhibits negligible capillary action. Under low flow rate conditions, the gas-liquid interface descends completely to the syringe bottom. However, with surfactant addition, the gas-liquid interface displacement is limited to approximately 6.6 mm. The reduction in surface tension facilitates the formation of small bubbles, thus diminishing the pressure requisite for bubble generation in the gas-supply chamber. A minor decrease in liquid level suffices to attain bubble release pressure.

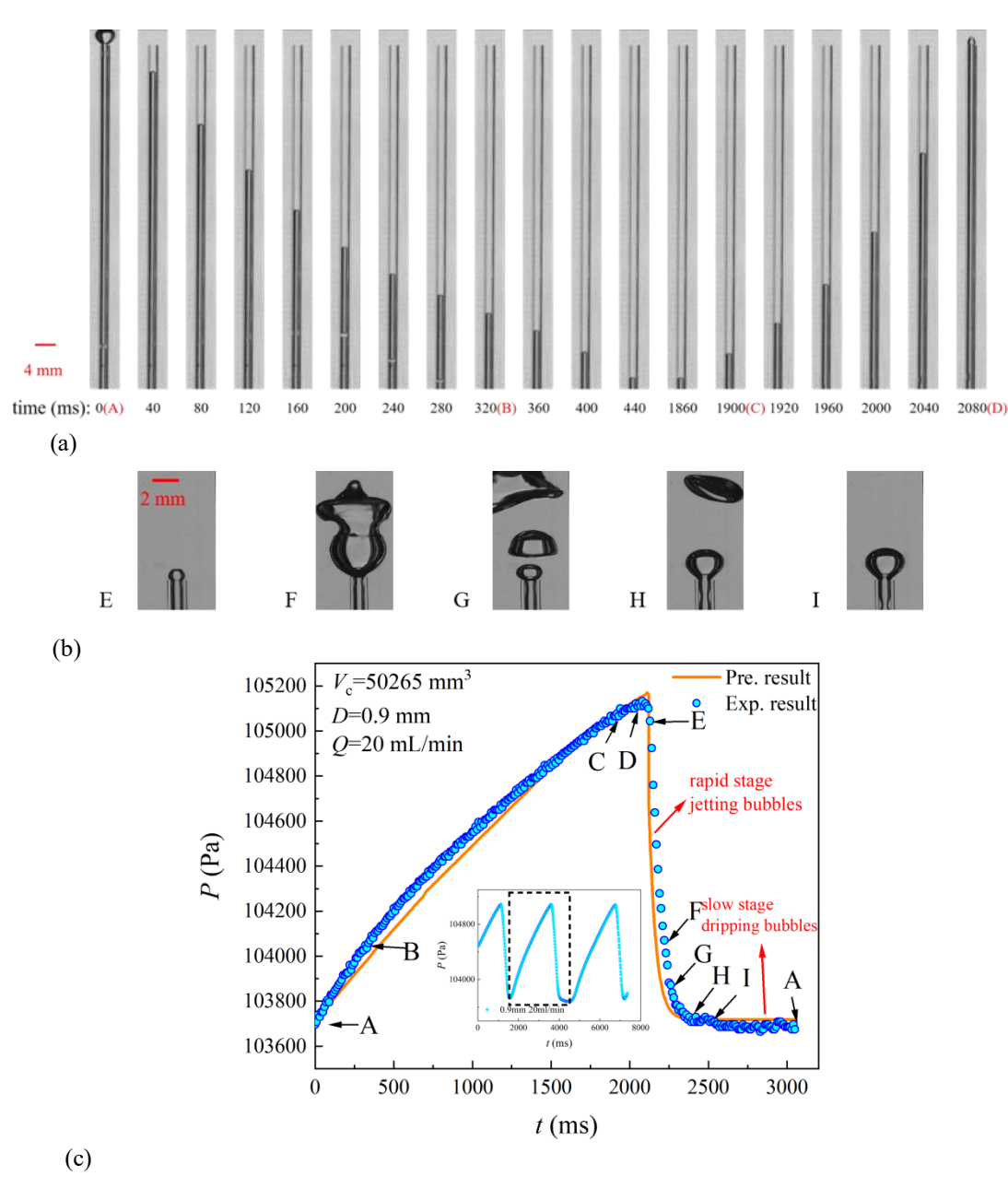


Fig. 10 Results in the case of N_2 , Q=20 mL/min, $V_c=50,265$ mm³, and D=0.9 mm. (a) Holding stage liquid column versus time. (b) Growth stage bubble versus time. (c) Comparison of the experimental data with the jet model results

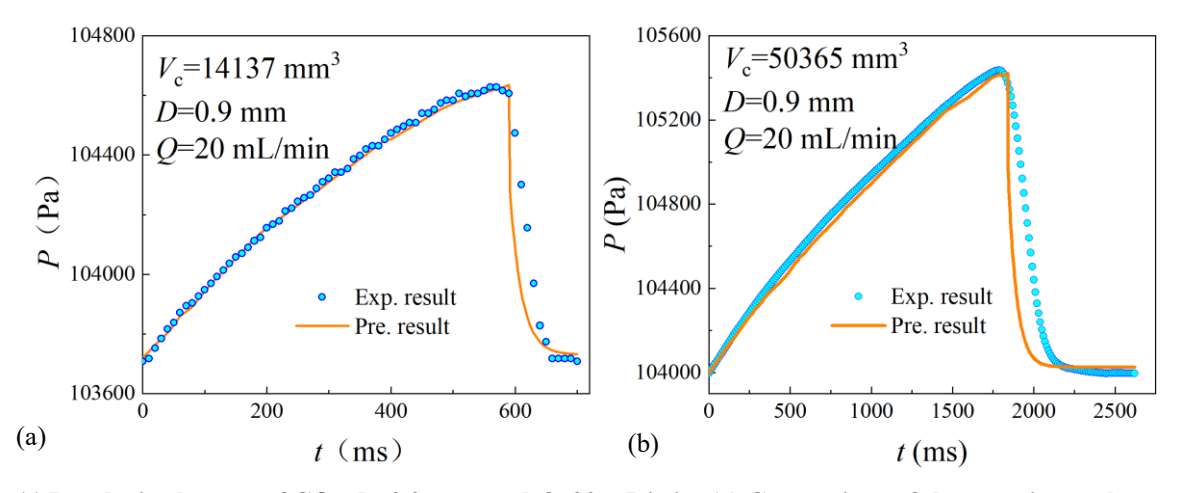


Fig. 11 Results in the case of CO₂, D=0.9 mm, and Q=20 mL/min. (a) Comparison of the experimental pressure profile with the jet model results at V_c =14,137 mm³. (b) Comparison of the pressure plot with the jet model results at V_c =50,265 mm³

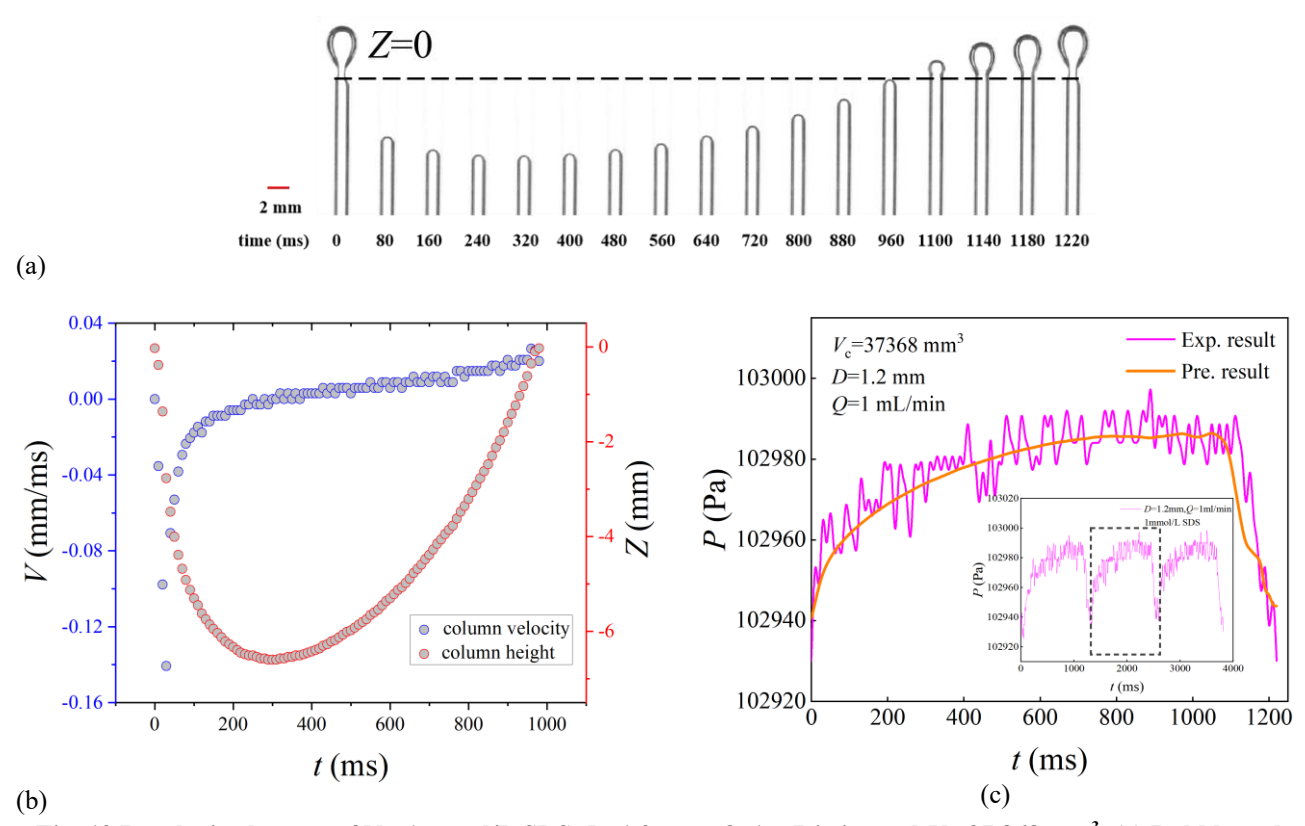


Fig. 12 Results in the case of N₂, 1 mmol/L SDS, D=1.2 mm, Q=1 mL/min, and V_c =37,868 mm³. (a) Bubble and column lowering visualization images. (b) Variation of column velocity and height with time. (c) Comparison of the experimental data with the drip model results

As established in the preceding analysis, the vertical displacement of the gas-liquid interface in the syringe serves as a key indicator for differentiating dripping-type and jetting-type generation modes. However, with surfactant present, despite the lowering of the gas-liquid interface, the bubble generation maintains the dripping-type behavior. As described by Eq. (4), variations in surface tension exert negligible influence on the drip model, while the pressure change in the gas chamber shows a primary dependence on the gas flow rate. The amplitude of the periodic pressure fluctuations observed in the experiment is approximately 60 Pa, as depicted in Fig. 12(c). Consistent with the Young-Laplace equation, the threshold differential pressure for bubble formation shows an inverse relationship with solution surface tension. Surfactant addition effectively reduces surface tension, thus promoting the formation of small, discrete bubbles. This phenomenon is in line with the drippingtype bubble-generation model (Babu & Das, 2018). Consequently, it can be concluded that the drip model can effectively predict the pressure fluctuations as long as the bubble generation follows the dripping type, regardless of whether column lowering occurs or not.

To substantiate these findings, a series of additional experiments were conducted. Following the addition of 1 mmol/L SDS surfactant, Fig. 13 demonstrates remarkable consistency between the experimental data with the drip model predictions across varying tube diameters and flow rates. These results conclusively demonstrate that the drip model can accurately predict

the pressure fluctuations associated with dripping-type bubble groups in surfactant-containing solutions.

Reynolds number (Re) is a dimensionless parameter describing the flow state in fluid dynamics, defined as the ratio of inertial force to viscous force. In bubble dynamics, Re is closely related to the generation, detachment, deformation, and motion behavior of bubbles. As clearly illustrated in Figs. 14(a) and 14(b), the bubble production frequency exhibits a consistent increase with increasing Reynolds number, independent of SDS concentration (1 mmol/L) or 10 mmol/L). However, in DI water, the frequency increase with higher Reynolds numbers occurs at a significantly reduced rate. The above results illustrate that the generation frequency of the bubble group is strongly influenced by the surface tension of the continuous phase solution, and stable periodic bubbles are more likely to be generated in the presence of surfactants. For SDS solutions, at elevated Reynolds numbers, bubble production becomes predominantly driven by inertial forces. Under these conditions, the drip model fails to accurately predict the pressure fluctuations within the bubble set. Consequently, the transition boundaries require precise determination through additional systematic experiments. Analysis of Figs. 14(a) and 14(b) reveals that the amplitude distribution of the bubble group shows greater concentration. The experimental results at 10 and 1 mmol/L show that the pressure amplitude generally decreases with increasing surfactant concentration. This is because an increased concentration reduces surface tension before the CMC is

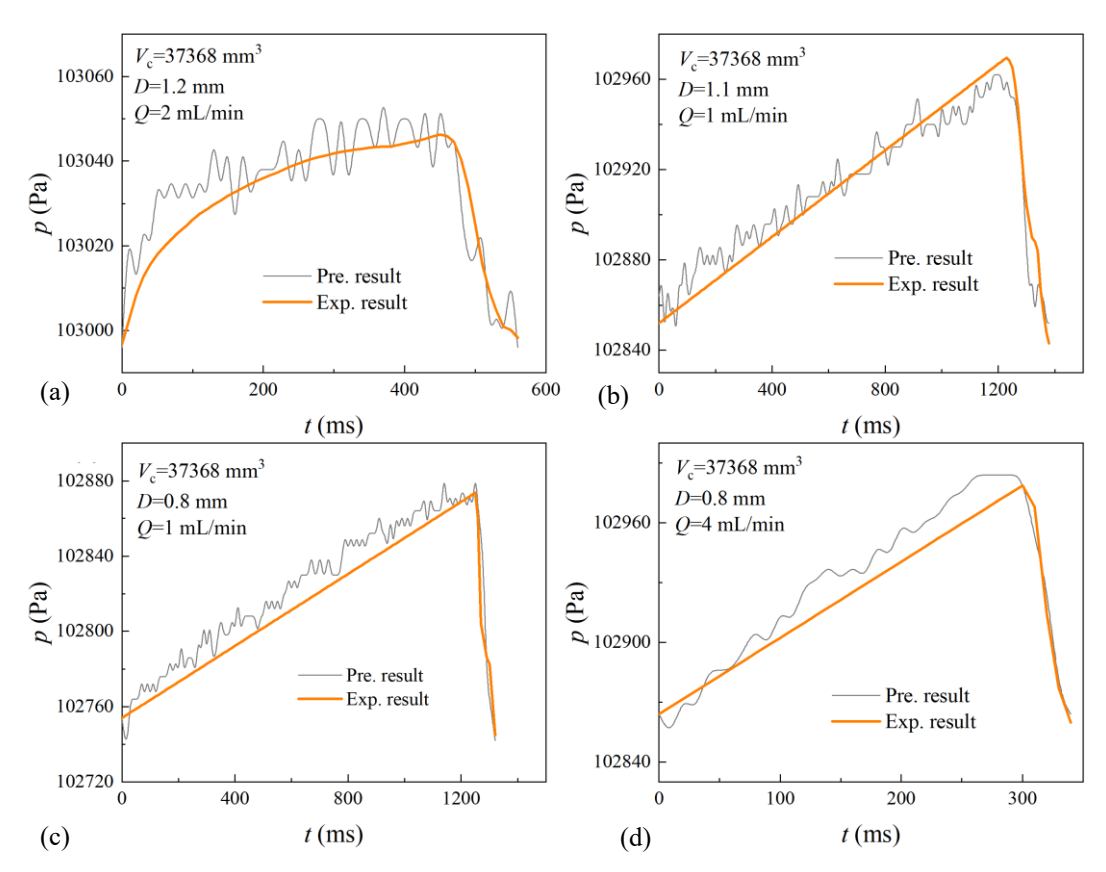


Fig. 13 Comparison of the experimental data with drip model results in the case of N₂ and 1 mmol/L SDS. (a) D=1.2 mm and Q=2 mL/min. (b) D=1.1 mm and Q=1 mL/min. (c) D=0.8 mm and Q=1 mL/min. (d) D=0.8 mm and Q=4 mL/min

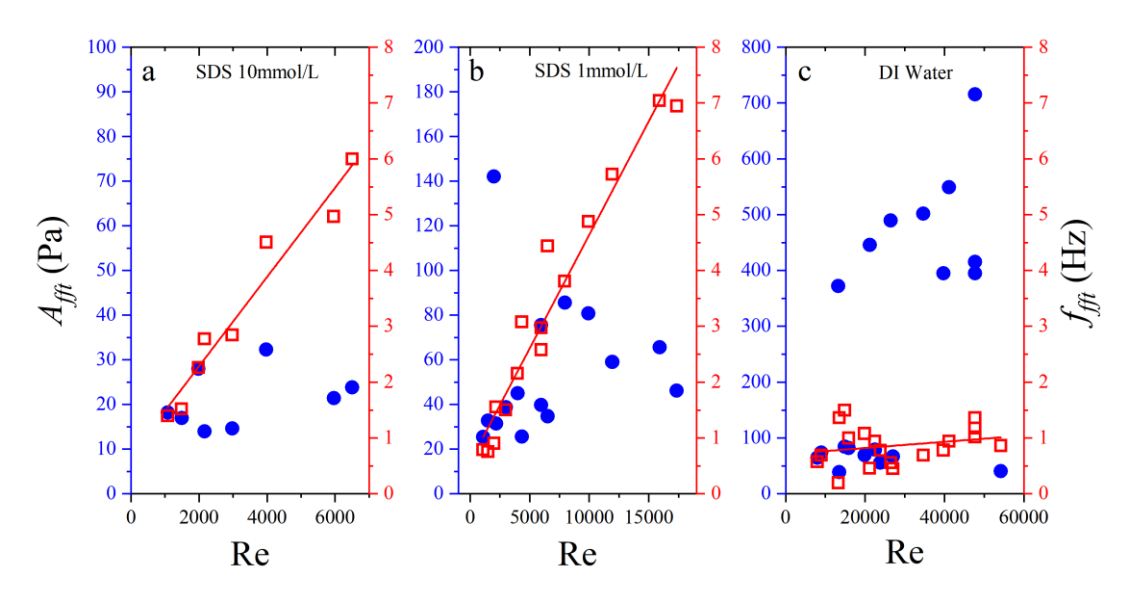


Fig. 14 Variation of bubble group amplitude and frequency with Reynolds number obtained after fast Fourier transform (FFT) treatment in the presence of surfactant under (a) 10 mmol/L SDS, (b) 1 mmol/L SDS, (c) DI water

reached, meaning that only a small change in pressure is required to form bubbles. As evident from Fig. 14(b), for a larger pipe diameter (1.2 mm) combined with a lower flow rate (2 mL/min), the amplitude increases substantially due to the liquid-column lowering phenomenon. In DI water systems, the amplitudes associated with small-diameter syringe needles maintain

consistent values in the absence of column lowering, whereas the amplitude exhibits a marked increase when the column lowering phenomenon is present. The experimental findings demonstrate that surfactant addition facilitates bubble generation while simultaneously mitigating the liquid-column drop phenomenon to a significant degree.

7. CONCLUSION

This study, through systematic analysis of multibubble generation dynamics and associated pressure fluctuation characteristics under mixed injection conditions, reveals the following key conclusions:

Systematic experimental observations identified two distinct bubble generation modes: the dripping type and the jetting-to-dripping type. When employing a 0.6-mm I.D. syringe in DI water experiments, no significant lowering of the liquid column was observed. The bubble formation occurred exclusively in the dripping-type regime, governed by the combined action of surface tension and shear force. Notably, even with surfactant addition, the bubbles maintained the dripping-type formation, albeit with a moderate lowering of the liquid level in the syringe. In contrast, using the 0.9-mm I.D. syringe resulted in a substantial reduction in the liquid level, accompanied by a jetting-to-dripping-type formation process that was predominantly driven by inertial forces.

- (1) For the dripping-type bubble formation process, the drip model demonstrates exceptional predictive capabilities. This prediction accuracy remains consistent for both N_2 and CO_2 , as well as across surfactant-containing solutions and DI water conditions. More specifically, the model exhibits remarkable precision in predicting the pressure variations associated with the formation of multiple bubbles.
- (2) The newly developed jet model has been rigorously validated through extensive comparison with experimental data. The validation results demonstrate the model's exceptional capacity to accurately predict the pressure fluctuations characteristic of jetting-to-dripping-type bubbles governed by inertial forces.

ACKNOWLEDGMENTS

This work was supported by the National Natural Science Foundation of China [No. 52006030]; the Shanghai Sailing Program [No. 18YF1400700]; the China Postdoctoral Science Foundation [No. 2018M641891]; and the Fundamental Research Funds for the Central Universities of China [No. 2232018D3-37].

CONFLICT OF INTEREST

No potential conflicts of interest were reported by the authors.

AUTHOR CONTRIBUTION

S. S. Lu: Conceptualization, Writing, Software. K. H. Xin: Conceptualization, Software. C. Dang: Resources, Supervision. H. W. Jia: Review, Editing, Funding acquisition.

DATA AVAILABILITY STATEMENT

The data that support the findings of this study are available from the corresponding author upon reasonable request.

REFERENCES

- Ambravaneswaran, B., Subramani, H. J., Phillips, S. D., & Basaran, O. A. (2004). Dripping-Jetting Transitions in a Dripping Faucet. *Physical Review Letters*, 93(3), 034501. https://doi.org/10.1103/PhysRevLett.93.034501
- Babu, R., & Das, M. K. (2018). Effects of surface-active agents on bubble growth and detachment from submerged orifice. *Chemical Engineering Science*, 179, 172–184. https://doi.org/10.1016/j.ces.2018.01.028
- Boubendir, L., Chikh, S., & Tadrist, L. (2020). On the surface tension role in bubble growth and detachment in a micro-tube. *International Journal of Multiphase Flow*, 124, 103196. https://doi.org/10.1016/j.ijmultiphaseflow.2019.1031 96
- Cano-Lozano, J. C., Bolaños-Jiménez, R., Gutiérrez-Montes, C., & Martínez-Bazán, C. (2017). On the bubble formation under mixed injection conditions from a vertical needle. *International Journal of Multiphase Flow*, 97, 23–32. https://doi.org/10.1016/j.ijmultiphaseflow.2017.07.0
- Chen, W., Huang, G., Hu, Y., Yin, J., & Wang, D. (2022). Experimental study on continuous spectrum bubble generator with a new overlapping bubbles image processing technique. *Chemical Engineering Science*, 254, 117613. https://doi.org/10.1016/j.ces.2022.117613
- Davidson, J. F., & Schüler, B. O. G. (1997). Bubble formation at an orifice in a viscous liquid. *Chemical Engineering Research and Design*, 75, S105–S115. https://doi.org/10.1016/S0263-8762(97)80008-1
- Dzienis, P., & Mosdorf, R. (2023). Liquid pressure fluctuations around a needle during bubble departures. *Meccanica*, 58(7), 1307–1313. https://doi.org/10.1007/s11012-023-01678-x
- Dzienis, P., Mosdorf, R., & Augustyniak, J. (2016). Liquid penetration inside glass nozzle during bubble departures in water. *Journal of Physics: Conference Series*, 745, 032048. https://doi.org/10.1088/1742-6596/745/3/032048
- Fu, J., Liu, Y., Zhang, C., Wang, C., Sun, S., Dong, H., She, Y., & Zhang, F. (2025). Microbial *in-situ* foam generation for enhanced oil recovery. *Physics of Fluids*, 37(1), 017175. https://doi.org/10.1063/5.0251406
- González-Sierra, N. E., Perez-Corte, J. M., Padilla-Martinez, J. P., Cruz-Vanegas, S., Bonfadini, S., Storti, F., Criante, L., & Ramos-García, R. (2023). Bubble dynamics and speed of jets for needle-free injections produced by thermocavitation. *Journal of Biomedical Optics*, 28(07). https://doi.org/10.1117/1.JBO.28.7.075004
- Goshima, T., Tsuji, Y., Mizuta, K., & Nii, S. (2022). Development of a fine bubble generator through the

- active control of gas chamber pressure. *Chemical Engineering Journal Advances*, 11, 100350. https://doi.org/10.1016/j.ceja.2022.100350
- Guo, W., He, B., Mao, H., Zhang, M., Hua, L., & Meng, Z. (2019). Mechanism of Bubble Formation in a Combined In-Mold Decoration and Microcellular Foaming Injection Molding Process. *Fibers and Polymers*, 20(7), 1526–1537. https://doi.org/10.1007/s12221-019-8777-3
- Haas, T., Schubert, C., Eickhoff, M., & Pfeifer, H. (2021). A Review of Bubble Dynamics in Liquid Metals. *Metals*, 11(4), 664. https://doi.org/10.3390/met11040664
- Ho, W.-S., Lin, W.-H., Verpoort, F., Hong, K.-L., Ou, J.-H., & Kao, C.-M. (2023). Application of novel nanobubble-contained electrolyzed catalytic water to cleanup petroleum-hydrocarbon contaminated soils and groundwater: A pilot-scale and performance evaluation study. *Journal of Environmental Management*, 347, 119058. https://doi.org/10.1016/j.jenvman.2023.119058
- Krishnamurthi, S., Kumar, R., & Kuloor, N. R. (1968). Bubble Formation in Viscous Liquids under Constant Flow Conditions. *Industrial & Engineering Chemistry Fundamentals*, 7(4), 549–554. https://doi.org/10.1021/i160028a004
- Kulkarni, A. A., & Joshi, J. B. (2005). Bubble Formation and Bubble Rise Velocity in Gas-Liquid Systems: A Review. *Industrial & Engineering Chemistry Research*, 44(16), 5873–5931. https://doi.org/10.1021/ie049131p
- Li, J., Bulusu, V., & Gupta, N. R. (2008). Buoyancy-driven motion of bubbles in square channels. *Chemical Engineering Science*, *63*(14), 3766–3774. https://doi.org/10.1016/j.ces.2008.04.041
- Li, M., Li, W., & Hu, L. (2020). Jet formation and breakup inside highly deformed bubbles. *International Journal of Heat and Mass Transfer*, 163, 120507. https://doi.org/10.1016/j.ijheatmasstransfer.2020.120
- Li, X., Shi, H., Wang, X., Hu, X., Xu, C., & Shao, W. (2022). Direct synthesis of graphene by blowing CO2 bubble in Mg melt for the seawater/oil pollution. *Journal of Alloys and Compounds*, 921, 165938. https://doi.org/10.1016/j.jallcom.2022.165938
- Mei, L., Chen, X., Liu, B., Zhang, Z., Hu, T., Liang, J., Wei, X., & Wang, L. (2023). Experimental Study on Bubble Dynamics and Mass Transfer Characteristics of Coaxial Bubbles in Petroleum-Based Liquids. ACS Omega, 8(19), 17159–17170. https://doi.org/10.1021/acsomega.3c01526
- Mi, S., Weldetsadik, N. T., Hayat, Z., Fu, T., Zhu, C., Jiang, S., & Ma, Y. (2019). Effects of the Gas Feed on Bubble Formation in a Microfluidic T-Junction: Constant-Pressure versus Constant-Flow-Rate Injection. *Industrial & Engineering Chemistry*

- Research, 58(23), 10092–10105. https://doi.org/10.1021/acs.iecr.9b01262
- Mirsandi, H., Smit, W. J., Kong, G., Baltussen, M. W., Peters, E. A. J. F., & Kuipers, J. A. M. (2020). Influence of wetting conditions on bubble formation from a submerged orifice. *Experiments in Fluids*, 61(3), 83. https://doi.org/10.1007/s00348-020-2919-7
- Mohseni, E., Chiamulera, M. E., Reinecke, S. F., & Hampel, U. (2022). Bubble formation from submillimeter orifices: Experimental analysis and modeling. *Chemical Engineering and Processing Process Intensification*, 173, 108809. https://doi.org/10.1016/j.cep.2022.108809
- Mohseni, E., Reinecke, S. F., & Hampel, U. (2023). Controlled bubble formation from an orifice through harmonic gas pressure modulation. *Chemical Engineering Journal*, 470, 143953. https://doi.org/10.1016/j.cej.2023.143953
- Mohseni, E., Ziegenhein, T., Reinecke, S. F., & Hampel, U. (2021). Bubble formation from sub-millimeter orifices under variable gas flow conditions. *Chemical Engineering Science*, 242, 116698. https://doi.org/10.1016/j.ces.2021.116698
- Oguz, H. N., & Prosperetti, A. (1993). Dynamics of bubble growth and detachment from a needle. *Journal of Fluid Mechanics*, 257(1), 111. https://doi.org/10.1017/S0022112093003015
- Park, Y., Lamont Tyler, A., & De Nevers, N. (1977). The chamber orifice interaction in the formation of bubbles. *Chemical Engineering Science*, *32*(8), 907–916. https://doi.org/10.1016/0009-2509(77)80077-8
- Quan, H., Li, J., Sun, J., Shi, G., Li, Y., Li, Y., Qiao, J., & Li, Y. (2025). Gas–liquid separation mechanisms and bubble dynamics in a helical axial multiphase flow pump. *Physics of Fluids*, *37*(2), 023334. https://doi.org/10.1063/5.0251497
- Ruiz-Rus, J., Bolaños-Jiménez, R., Sevilla, A., & Martínez-Bazán, C. (2020). Bubble pressure requirements to control the bubbling process in forced co-axial air-water jets. *International Journal of Multiphase Flow*, 133, 103467. https://doi.org/10.1016/j.ijmultiphaseflow.2020.103467
- Shahidani, A., Mokhtari-Dizaji, M., & Shankayi, Z. (2024). The effect of dual-frequency sonication parameters on the oscillatory behavior of microbubble in blood fluid. *Physics of Fluids*, 36(11), 111912. https://doi.org/10.1063/5.0236627
- Wei, C., Hao, R., Zhu, D., Khudayberdi, N., & Liu, C. (2025). Improving the hydraulic performance of aerated irrigation pipeline. *Physics of Fluids*, *37*(2), 023333. https://doi.org/10.1063/5.0249475
- Xiang, S., Jian, Z., Kherbeche, A., & Thoraval, M. J. (2022). Experimental study of single bubble rising near vertical wall in hele-shaw cell. *Chemical*

- Engineering Science, 255, 117647. https://doi.org/10.1016/j.ces.2022.117647
- Yang, B., Jafarian, M., Freidoonimehr, N., & Arjomandi, M. (2023). Controlled Bubble Formation From a Microelectrode Single Bubble Generator. *Journal of Fluids Engineering*, 145(11), 111401. https://doi.org/10.1115/1.4062962
- Yang, Y., Shan, M., Kan, X., Duan, K., Han, Q., & Juan, Y. (2023). Thermodynamic effects of gas adiabatic index on cavitation bubble collapse. *Heliyon*, 9(10), e20532. https://doi.org/10.1016/j.heliyon.2023.e20532
- Yu, X., Wu, Y., Li, Y., Yang, Z., & Ma, Y. (2020). The formation of satellite droplets in micro-devices due to the rupture of neck filament. *Chemical Engineering Research and Design*, 153, 435–442. https://doi.org/10.1016/j.cherd.2019.11.016

- Zhang, J., Yu, Y., Qu, C., & Zhang, Y. (2017). Experimental study and numerical simulation of periodic bubble formation at submerged micronsized nozzles with constant gas flow rate. *Chemical Engineering Science*, 168, 1–10. https://doi.org/10.1016/j.ces.2017.04.012
- Zhao, K., & Sun, L. (2024). Superwetting Capillary Tubes: Surface Science under Confined Space. *Langmuir*, 40(18), 9319–9327. https://doi.org/10.1021/acs.langmuir.3c04044
- Zhou, Y., Yang, Y., Zhu, X., Ye, D., Chen, R., & Liao, Q. (2021). Bubble-trap layer for effective removing gas bubbles and stabilizing power generation in direct liquid fuel cell. *Journal of Power Sources*, 507, 230260. https://doi.org/10.1016/j.jpowsour.2021.230260